

ASME Journal of Heat and Mass Transfer Online journal at:

https://asmedigitalcollection.asme.org/heattransfer



Dylan Paap

Alan Levin Department of Mechanical and Nuclear Engineering, Kansas State University, 3002 Rathbone Hall, 1701B Platt Street, Manhattan, KS 66506 e-mail: dylanpaap@ksu.edu

Benjamin Weinhold

Alan Levin Department of Mechanical and Nuclear Engineering, Kansas State University, 3002 Rathbone Hall, 1701B Platt Street, Manhattan, KS 66506 e-mail: bweinhold@ksu.edu

Partha Pratim Chakraborty

Alan Levin Department of Mechanical and Nuclear Engineering, Kansas State University, 3002 Rathbone Hall, 1701B Platt Street, Manhattan, KS 66506 e-mail: parthapratim@ksu.edu

Will VandenBos

Alan Levin Department of Mechanical and Nuclear Engineering, Kansas State University, 3002 Rathbone Hall, 1701B Platt Street, Manhattan, KS 66506 e-mail: vandenbo@ksu.edu

Melanie M. Derby

Mem. ASME
Alan Levin Department of Mechanical and
Nuclear Engineering,
Kansas State University,
3002 Rathbone Hall,
1701B Platt Street,
Manhattan, KS 66506
e-mail: derbym@ksu.edu

Evaporation Mechanisms and Heat Transfer in Porous Media of Mixed Wettabilities With a Simulated Solar Flux and Forced Convection Through the Media

An experimental apparatus was designed to study the impacts of wettability on evaporation of water from Ottawa sand. Evaporation rates were measured for: (1) a 5.7-cm-thick layer of hydrophilic Ottawa sand; (2) a 5.7-cm-thick layer with 12% hydrophobic content, consisting of a 0.7-cm-layer of n-Octyltriethoxysilane-coated hydrophobic sand buried 1.8 cm below the surface of hydrophilic sand; and (3) a 5.7-cm-thick layer with mixed wettabilities, consisting of 12% n-Octyltriethoxysilane-coated hydrophobic sand mixed into hydrophilic sand. The sand-water mixtures experienced forced convection above and through the sand layer, while a simulated solar flux (i.e., 112±20 W/m²) was applied. Evaporation from homogeneous porous media is classified into the constant-rate, falling-rate, and slow-rate periods. Wettability affected the observed evaporation mechanisms, including the transition from constant-rate to falling-rate periods. Evaporation entered the falling-rate period at 12%, 20%, and 24% saturations for the all hydrophilic sand, hydrophobic layer, and hydrophobic mixture, respectively. Wettability affected the duration of the experiments, as the all hydrophilic sand, hydrophobic layer, and hydrophobic mixture lasted 17, 20, and 26 trials, respectively. Both experiments with hydrophobic particles lasted longer than the all hydrophilic experiment and had shorter constant-rate evaporation periods, suggesting hydrophobic material interrupts capillary action of water to the soil surface and reduces evaporation. Sand temperatures suggest more evaporation occurred near the test section inlet for higher saturations and the hydrophobic layer experienced more evaporation occur near the outlet. Evaporation fluxes were up to 12× higher than the vapor diffusion flux due to enhanced vapor diffusion and forced convection. [DOI: 10.1115/1.4065608]

Keywords: porous media, liquid island, liquid bridge, convection, hydraulic conductivity

1 Introduction and Literature Review

The Ogallala Aquifer is a critical source of water for crops and livestock in the U.S. Central High Plains [1], which in 2015 supplied approximately 30% of the water for irrigated agriculture in the U.S. [2]. Due to the semi-arid climate of this region, limited rainfall (e.g., 0.33–0.74 m of precipitation annually [3]) is available, and McGuire

¹Corrsponding author.

Contributed by the Heat Transfer Division of ASME for publication in the JOURNAL OF HEAT AND MASS TRANSFER. Manuscript received September 22, 2023; final manuscript received April 25, 2024; published online June 6, 2024. Assoc. Editor: Brian D. Iverson.

[4] determined the aquifer declined by more than 45 m in parts of western Kansas from 1950 to 2013. Reducing the evaporation from soil—a complex, porous media—is one approach to conserving water in the food, energy, and water nexus.

Evaporation from homogeneous porous media occurs in three stages: constant-rate, falling-rate, and slow-rate periods [5–9]. In the first stage, nearly constant and relatively high evaporation rates are observed compared to the subsequent stages. The constant-rate period includes water being evaporated from the top surface by convection, and water is supplied to the top surface by capillary action [10]. Davarzani et al. [11] concluded that constant-rate evaporation is driven by atmospheric conditions (e.g., radiation, wind, air temperature, and humidity [9]). The falling-rate period of evaporation depends on the saturation of the porous media (i.e., the ratio of the volume of water to the total volume of the void space [12]). An et al. [13] determined that increasing the amount of sand in a soil mixture extended the length of the constant-rate period of evaporation. Chakraborty et al. [6] determined that the constant-rate period of evaporation was negligible due to the size and homogeneity of their porous media, which limited capillary action. Once the soil partially dries out, thus breaking capillary flows, the evaporation rate decreases continuously [6]; the falling-rate period begins abruptly, once the gravitational and viscous resistances overcome the capillary forces of the liquid in the porous media [14].

The slow-rate period evaporation rate is considerably lower than the previous stages (e.g., <10% of the constant-rate period [7]), is affected by porous media characteristics (e.g., porosity, particle size, compaction, etc.), and occurs at lower saturations [7]. Philip and De Vries [15] measured vapor transport 3.6–18× higher than vapor diffusion predicted using Fick's law. Philip and De Vries [15] suggested this enhancement, named enhanced vapor diffusion, was due to temperature gradients and condensation and evaporation across liquid bridges or islands that formed between particles in a porous media. Cary [16] experimentally determined that temperature gradients also enhance vapor transport, and Jury and Letey Jr [17] suggested that water vapor movement can be a function of temperature alone, independent of water content, over a significant saturation range.

Altering the wettability of porous media impacts evaporation mechanisms [6,10,14,18–20] by interrupting moisture transport to the surface, and although most soils are hydrophilic [21], some soils may be naturally hydrophobic as a result of mineral coatings [22,23], organic material [23–25], or waxes generated by forest fires [26,27]. When heated, hydrophobic, organic matter can coat adjacent soil particles, thereby increasing water repellency [20], which may impede moisture penetration and create runoff [28,29]. In the laboratory, hydrophobicity is often promoted with chemical coatings (e.g., a silane solution on sand [30,31]).

Shokri et al. [14] experimentally determined that hydrophobic layers in a hydrophilic, porous media column reduced the total evaporation. A column with a 0.007-m layer of hydrophobic material, buried 0.018 m below the surface, reduced evaporation by approximately 64% compared to a completely hydrophilic column. Shokri et al. [19] determined that mixing 10% hydrophobic material or more into a hydrophilic porous media reduced the constant-rate evaporation period. The falling-rate evaporation period began with a drying front depth of 0.08 m and 0.13 m, respectively, for a column with 10% hydrophobic and a completely hydrophilic column, indicating more water evaporated from the hydrophilic column during the constant-rate evaporation period. Chakraborty et al. [6] investigated evaporation of water from 6-cm-height beakers containing hydrophilic glass beads or hydrophobic Teflon beads. Experiments with Teflon beads entered the slow-rate period 20 h prior to the beaker of glass beads and the drying front depths indicated more water remained in the hydrophobic Teflon column.

The research objectives of this study are to investigate the impacts of hydrophobicity on evaporation mechanisms from hydrophilic Ottawa sand. Experiments include all hydrophilic Ottawa sand, and two cases of mixed hydrophilic and silane-coated hydrophobic sand (i.e., a 12% hydrophobic layer buried in hydrophilic sand, and a 12%

hydrophobic mixture). This study differs from previous research by scaling-up compared to previous studies [6,14,18,19] from beaker-scale to a 0.838-m-long, 0.229-m-wide, and 0.057-m-tall test section with 16 kg of sand. This study also combines the components of convection (i.e., constant air flow above and through the sand sample) and a solar heat flux, which were not paired in previous research.

2 Experimental Design

2.1 Experimental Apparatus. To study the impacts of wettability on evaporation under a simulated solar flux, with forced convection above and below-and, thus, through-the porous media, an air-tight test section was required that could suspend the sand-water mixture above a chamber with flowing, dry air and allow a solar heat flux (Fig. 1). The evaporation rate was determined through a mass balance on the flows entering and leaving the test section. The test section was constructed out of 0.006-m-thick aluminum plates welded and bolted together with rubber gaskets (McMaster 5812T35). A metal, crossed structure supported the sand layer (Fig. 2) with a single layer of nylon, semipermeable membrane (EMD Millipore NY6000010). The membrane was attached with adhesive tape in order to hold the sand layer and allow air to pass through the sand. The porous media studied was a layer of 0.057-mthick Ottawa sand. Clear polycarbonate was attached to the side and top of the test section with industrial adhesive (Loctite AA H8000) that permitted viewing of the sand and a solar heat flux applied to the sand's surface. Reflective heat tape (McMaster 76035A43) on the edges of the polycarbonate window shielded the adhesive from the solar simulator (Fig. 2). Holes were drilled in the side of the test section for nine thermocouples (Omega TMQSS-062 U-6) to measure the temperature of the porous media at locations A, B, and C (i.e., 0.079 m, 0.419 m, and 0.759 m from the inlet, respectively), and at depths of 0.008 m, 0.02 m, and 0.035 m, at positions 1, 2, and 3, respectively.

Building supply air at 827 kPa was regulated and dried to near-zero relative humidity in a desiccator (Sharpe 6760, Dryaire Desiccant System Minneapolis, MN). The air flow was heated to the required temperature in a heat exchanger submerged in a water bath (Neslab RTE-211A, Portsmouth, NH). Subsequently, at a tee junction, the air was divided to travel above and below the sand layer at flow rates of 2.0×10^{-4} kg/s, respectively. Air flows were controlled by multiple valves (Swagelok Valve SS-45S8, Solon, OH). Air pressure and volumetric flowrate measurements were recorded by pressure transducers (Omega PX309-100G5V, Norwalk, CT) and volumetric flow meters (Omega FMA-1609A, Norwalk, CT); mass flow rates were calculated in Engineering Equation Solver.

The two inlet flows (labeled 0 and 1 on Fig. 1) passed through humidity sensors (Omega HX200HR, Norwalk, CT) and thermocouple probes (Omega TMQSS-0125 U-6, Norwalk, CT). After flowing through the test section, moist air passed through a Swagelok valve to ensure mixing, and temperature and relative humidity were recorded at the outlet ((2) on Fig. 1). Data were acquired in LABVIEW. A heated blanket was wrapped around the test section for heating during startup and to insulate throughout trials (McMaster 3571K31, Carr Elmhurst, IL); additional fiberglass insulation was installed to reduce heat loss. The entire apparatus was placed on a scale (McMaster 1852T85, Carr Elmhurst, IL; capacity of 250±0.01 kg) to measure the gravimetric water content.

Seventeen halogen lights (Sylvania 14823, Wilmington, MA) were placed 0.25 m above the sand layer and were cooled by five fans; heat fluxes were measured using a LICOR, Lincoln, NE light meter and pyranometer (LI-250A and PY106695, respectively). In a review of the penetration of light through soils, Tester and Morris [32] noted that for most soils, penetration of light beyond 4–5 mm is not significant, and longer wavelengths penetrate deeper than shorter wavelengths. Baranoski et al. [33] conducted modeling and experiments to determine the transmittance of 400–1000 nm light through samples of natural sand. Depending on the sand and wavelength, at depths of 3 mm below the surface, transmittance was

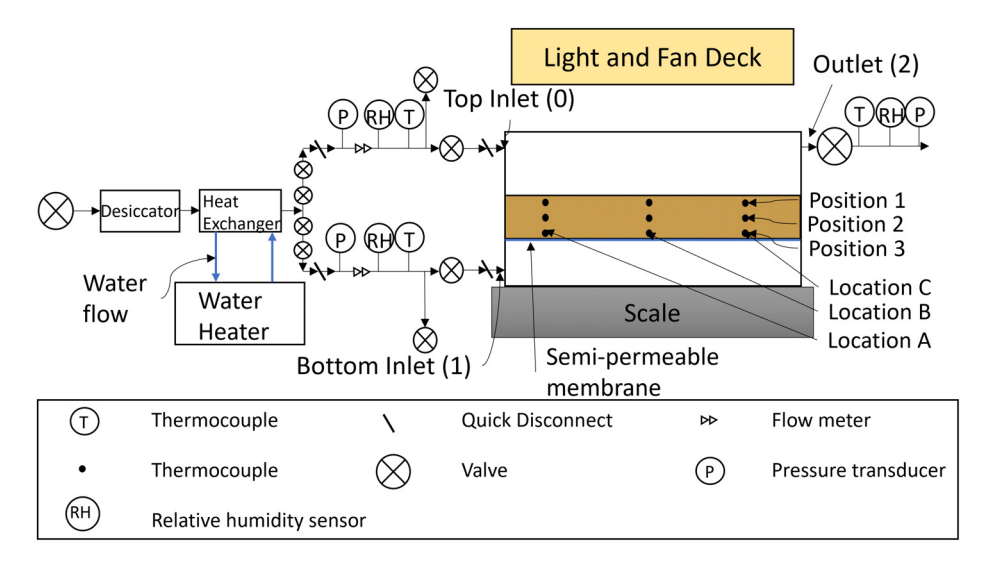


Fig. 1 Schematic of the experimental apparatus designed to conduct mass balances on the two inlet flows and single exit flow to determine evaporation rates; dry air enters through inlet 0 and inlet 1, and the air travels above and below/through the sand layer, respectively

low (i.e., 0–3.5%). Thus, it is likely that most of the incident solar radiation is absorbed by the first few millimeters of the sand. Of the three experimental cases, the all hydrophilic Ottawa sand and hydrophobic layer both have hydrophilic sand at the surface; in the hydrophobic mixture, the top surface is 12% hydrophobic material, which may affect absorption of the incident radiation.

2.2 Sand Contact Angles and Preparation. The experiments used hydrophilic and silane-coated natural silica ASTM 20-30 Ottawa sand (Humboldt; H-3820BX). Per Humboldt [34], the sand is graded to retain 98% on a 150-μm sieve, 75% on a 300-μm sieve, 30% on a 425-μm sieve, and 2% on a 600-μm sieve. The sand has a well-characterized particle size distribution and supports multiple ASTM and AASHTO standards. Ottawa sand was experimentally determined by McGaw [35] to have a thermal conductivity of 0.324 W/m K for dry sand; conductivity increased as the saturation of the sand increased. Tarnawski et al. [36] measured thermal conductivity of Ottawa sand. The thermal conductivity ranged from 0.284 W/m K to 0.323 W/m K for the temperature range of 25–70 °C when completely dry. Kersten [37] determined that the specific heat capacity of Ottawa sand ranged from 628 J/kg K to 795 J/kg K over temperatures ranging from −18 °C to 60 °C.

Plain Ottawa sand was heated in a convection oven at 105 °C for one hour to eliminate microbial activity or plants. The sand was affixed to double sided tape on a glass slide and its contact angle was measured to be 23 deg using a goniometer (First Ten Angstroms 206140; Fig. 3(a)). Hydrophobic Ottawa sand was created through coating it with 10% n-Octyltriethoxysilane (Fisher Scientific AC338081000) and 90% isopropanol, by volume, based on the procedure developed by Truong et al. [31]. Sand was prepared by rinsing with de-ionized water three times and drying in an oven at

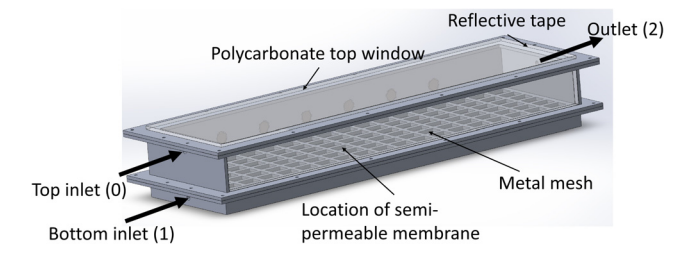


Fig. 2 Isometric view of the test section showing the inlets and single outlet; a semipermeable membrane sits atop the metal mesh in order to support the sand–water mixture

 $105\,^{\circ}\text{C}$ for a minimum of 24h. Sand was added to the silane-isopropanol solution until a thin film of the solution mixture was still present above the sand. The sand and solution were stirred periodically throughout the 48-h coating process. The sand was removed from the solution and rinsed with de-ionized water three times, and then dried in an oven at $40\,^{\circ}\text{C}$. The contact angles indicate the silane-coated sand is hydrophobic, with contact angles of $109-117\,\text{deg}$ (Fig. 3(b)).

Sand was placed into the test section completely dry, leveled, and the mass was recorded to estimate the amount of sand needed to fill the test section; this amount was increased by 10% for each experimental preparation to permit additional sampling to check the saturation. In a container, water was added by mass to the sand for the desired saturation percentage [12]. Preliminary experiments without a solar simulator suggested that the falling rate period of evaporation did not occur until below 50% saturation and using a lower starting saturation prevented seepage through the semipermeable membrane, which occurred at saturations over 80%. The saturations studied in this work are comparable to field capacities (i.e., the amount of water remaining in soil after initial drainage due to gravity) of sandy soils. Ratliff et al. [38] measured volumetric field capacities of 0.10, 0.16, and 0.21 $m_{\text{water}}^3/m_{\text{soil}}^3$ for sand, loamy sand, and sandy loam soil types, respectively. This corresponds to the gravimetric water content, w, which was below 0.081 kg_w/kg_s for each experiment in this study.

With hydrophobic sand, there were challenges with water penetrating the hydrophobic porous media, and more mixing was required than for the hydrophilic sand. The sand—water mixture was stirred for a minimum of one minute to distribute the water throughout the sand. The scale was tared and the sand—water mixture was added in three layers to prevent air pockets. The sand was smoothed with the leveling bar and the excess, partially saturated sand was fully dried to calculate the saturation uncertainty. The test section was then sealed using a torque wrench.

2.3 Operating Procedure. Due to the thermal mass of the chamber, temperature data were recorded to ensure measured evaporation rates occurred at steady-state. The top air flow was opened to the test section and the heated blanket was set to 38 °C to raise the test section above the dewpoint temperature in order to prevent condensation inside the test section. Once the target inlet air temperatures were reached (i.e., 28–31.5 °C); the air lines entering the test section were disconnected at quick connects, the heated blanket was turned off, and the mass of the test section was recorded (i.e., the initial starting mass of the trial). Air lines were reconnected

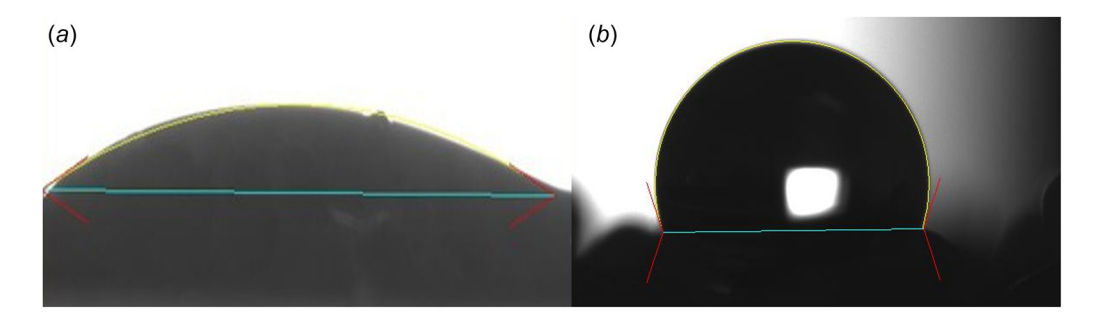


Fig. 3 Measured contact angles of: (a) 23 deg on plain Ottawa sand and (b) 109 deg (right side) and 117 deg (left side) on silane-coated Ottawa sand

to the test section and lights were activated to supply an average heat flux value for all locations within the test section of $112\pm20~\text{W/m}^2$ (two standard deviations). The heated blanket was adjusted to permit light to enter the test section but remained on the scale for mass measurement. Trials were recorded in LABVIEW for 45–75 min after the lights were activated, depending upon the temperature of the outlet flow from the test section. Calculations were performed using Engineering Equation Solver. Mass flow rates were calculated using temperature, pressure, and relative humidity for the inlets and outlet to the test section. The final ending mass of the test section was recorded and the average mass for the trial was calculated.

2.4 Data Reduction. Evaporation rates were calculated using the mass balance of water into and out of the test section

$$\dot{m}_{\mathrm{wr}} = \frac{\partial m_{\mathrm{wr}}}{\partial t} = (\dot{m}_{a0} + \dot{m}_{a1})\omega_2 - (\dot{m}_{a0}\omega_0 + \dot{m}_{a1}\omega_1) \tag{1}$$

where $\dot{m}_{\rm wr}$ is the evaporation rate in kg_{water}/s from the porous media; $m_{\rm wr}$ is the mass storage in the test section; t is the time; \dot{m}_{a0} and \dot{m}_{a1} are the mass flow rates of air through top and bottom inlets in kg/s, respectively; and ω_0 , ω_1 , and ω_2 are the humidity ratios at the top inlet, bottom inlet, and outlet, respectively. Steady-state conditions were defined based on the air outlet temperature, which formed an asymptote that approached a constant temperature (Fig. 4). Data were collected from a quasi-steady section of the temperature curve; the values of the temperature changed by 0.01-0.36 °C over a 500-second period during steady-state. The average saturation percentage for each trial is calculated by measuring mass before and after drying [13,39], (i.e., gravimetric water content [12] or gravimetric wetness [40]). Initially, a mass of sand was measured in a five-gallon

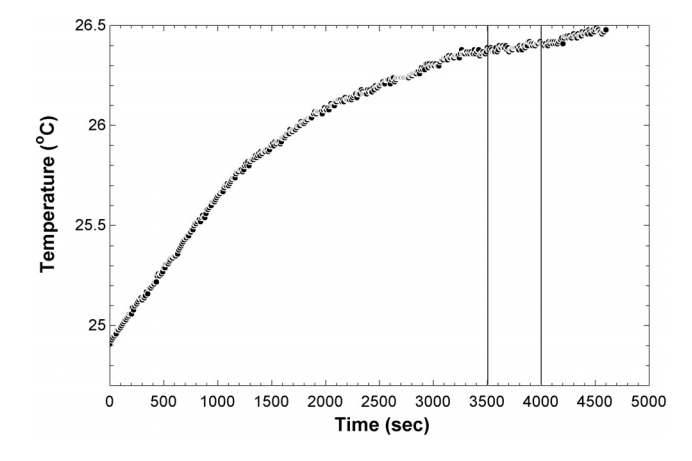


Fig. 4 The transient, outlet air temperature was used to determine steady-state conditions; in this case, data were collected from 3500 to 4000 s, as indicated by vertical lines, and the average evaporation rate collected from the same 500-s time interval

container along with an initial mass of water and the container saturation ratio was calculated using the equation

$$S_c = \frac{w_c G_{\text{specific}}}{e} = \frac{\frac{m_{\text{wr}c}}{m_{sc}} G_{\text{specific}}}{e}$$
 (2)

where S_c is the saturation ratio, w_c is the gravimetric water content of the sand—water mixture kg_{water}/kg_{sand} , m_{wrc} is the mass of water, m_{sc} is the mass of sand added, and G_s is the specific gravity, defined as 2.65 for Ottawa sand [41], and subscript c refers to samples in the container. Void ratio of Ottawa sand depends on the porosity. Ottawa sand was selected as it has been experimentally determined to minimally change in porosity with compression

$$e = \frac{n}{1 - n} \tag{3}$$

where e is void fraction and n is porosity, of which 0.35 is an average value for Ottawa sand [42,43]. El Ghoraiby et al. [42] determined the porosities for Ottawa sand ranging from 0.33 to 0.38 with an average of 0.35 using pluviation, consolidation, and shearing compaction methods. After mixing in the container, the sand—water mixture was loaded into the test section, and the mass measurement recorded in the test section was the mixture alone. The water content of the sand was assumed to remain the same from the container

$$m_{\rm sts} = \frac{m_{\rm int\,s}}{1 + w_c} \tag{4}$$

where $m_{\rm sts}$ is the mass of sand placed into the test section and $m_{\rm int,s}$ is the total mass initially placed into the test section. Once placed into the test section, the mass of sand does not change. Therefore, the mass of water for each individual trial is found by subtracting the mass of sand in the test section from the total mass of sand and water mixture of the test section for that individual trial, allowing for the calculation of the saturation ratio for that trial

$$m_{\rm wrtr} = m_{\rm tr} - m_{\rm sts} \tag{5}$$

$$S_{\rm tr} = \frac{\frac{m_{\rm wrtr}}{m_{\rm sts}} G_{\rm specific}}{e} \tag{6}$$

where $S_{\rm tr}$ is the saturation ratio, $m_{\rm wrtr}$ is the mass of water in the test section, $m_{\rm tr}$ is the mass of the test section, and subscript tr corresponds to each individual trial.

2.5 Uncertainty Analysis. The primary uncertainty for the measurements of air flow was due to the uncertainty of the instrumentation: $\pm 0.8\%$ of the reading plus $\pm 0.2\%$ of the full scale for the volumetric flow meters, $\pm 0.2\,^{\circ}\mathrm{C}$ for the calibrated thermocouples, $\pm 1\%$ RH for the relative humidity sensors, and $\pm 0.25\%$ full scale for the pressure transducers. The uncertainty of the evaporation rate was a combination of the uncertainty in the sensors used to calculate the mass flow rates of air and the humidity ratios used to calculate evaporation rate [44]

$$\Omega_{\dot{m}_{\rm wr}} = \sqrt{\left(\frac{\partial \dot{m}_{\rm wr}}{\partial \dot{m}_{a0}} \Omega_{\dot{m}_{a0}}\right)^2 + \left(\frac{\partial \dot{m}_{\rm wr}}{\partial \dot{m}_{a1}} \Omega_{\dot{m}_{a1}}\right)^2 + \left(\frac{\partial \dot{m}_{\rm wr}}{\partial \omega_0} \Omega_{\omega_0}\right)^2 + \left(\frac{\partial \dot{m}_{\rm wr}}{\partial \omega_1} \Omega_{\omega_1}\right)^2 + \left(\frac{\partial \dot{m}_{\rm wr}}{\partial \omega_2} \Omega_{\omega_2}\right)^2}$$
(7)

where $\Omega_{\dot{m}_{wr}}$ is the uncertainty in the mass flowrate of water; $\Omega_{\dot{m}_{a0}}$ and $\Omega_{\dot{m}_{a1}}$ are the uncertainties of the mass flowrate of air at inlet 0 and 1, respectively; Ω_{ω_0} , Ω_{ω_1} , and Ω_{ω_2} are the uncertainties of the humidity ratio at inlet 0, inlet 1, and outlet 2, respectively. The uncertainties of humidity ratio were calculated using the upper uncertainty of temperature, the lower uncertainty of pressure, and the upper uncertainty in the relative humidity. The uncertainty for the mass flowrate of air is

$$\Omega_{\dot{m}_a} = \sqrt{\left(rac{\partial \dot{m}_a}{\partial
ho} \Omega_{
ho}\right)^2 + \left(rac{\partial \dot{m}_a}{\partial \dot{v}} \Omega_{\dot{v}}\right)^2}$$
 (8)

where Ω_{ρ} is the uncertainty of the density of air and $\Omega_{\dot{\nu}}$ is the uncertainty of the volumetric flowrate.

The value of the initial saturation of the test section was the most significant source of uncertainty for the saturation ratio. A target saturation for the experiments was calculated for the sand and water in the mixing container. The excess sand–water mixture was removed, and the mass of excess sand and water was determined. The difference between the water content of the container and the uncertainty water content was used for the uncertainty in the water content for a particular experiment, $\Omega_{\rm w}$

$$\Omega_{w} = \left| \frac{m_{\text{wr}\,u}}{m_{su}} - \frac{m_{\text{wr}\,c}}{m_{sc}} \right| \tag{9}$$

where m_{su} is the uncertainty mass of sand in the test section found by subtracting the mass of excess sand from the mass of sand in the container and m_{wru} is the uncertainty mass of water, found using similar methods as uncertainty mass of sand.

The uncertainty of the saturation for each trial, Ω_{S_v} , is due to the uncertainty in the scale measurement of the total mass of sand—water mixture of each trial, Ω_{m_v} , and initial mass placed into the chamber, $\Omega_{m_{\rm int}}$, which were $\pm 0.01\,{\rm kg}$, and the uncertainty of the water content in the test section, Ω_w

$$\Omega_{S_{tr}} = \sqrt{\left(\frac{\partial S}{\partial m_{tr}}\Omega_{m_{tr}}\right)^2 + \left(\frac{\partial S}{\partial m_{ints}}\Omega_{m_{ints}}\right)^2 + \left(\frac{\partial S}{\partial w}\Omega_{w}\right)^2} \quad (10)$$

The experiments that included hydrophobic sand included a larger value of uncertainty in the water content due to reduced water infiltration, as there is reduced water penetration and increased amount of runoff in hydrophobic soils [21].

3 Results and Discussion

Evaporation experiments were conducted for three cases: (1) all hydrophilic Ottawa sand; (2) a 12% hydrophobic layer with hydrophobic Ottawa sand 0.007-m-thick, 0.018 m below the surface of hydrophilic Ottawa sand, termed "hydrophobic layer"; and (3) a 12% mixture of hydrophobic sand with hydrophilic Ottawa sand, termed "hydrophobic mixture." Section 3.1 describes the results of the mass flow validation of the test section. Sections 3.2–3.5 describe the results of each evaporation study, the vapor diffusive flux, temperature profiles, and nondimensional numbers, respectively.

3.1 Mass Flow Validation. A mass balance was calculated by measuring dry air flows into and out of the test section, with no sand present, to verify the test section was sealed. The temperature, pressure, and relative humidity for both inlets and the outlet were recorded in Labview, along with the volumetric flowrate of both inlets. The outlet volumetric flow was recorded at the outlet with a rotameter only for these validation trials (McMaster 3281K15, $\pm 6\%$ FS; Fig. 5), thereby resulting in a higher test section internal pressure during validation experiments. Agreement was within $\pm 10\%$ at pressures below 111 kPa. The point which deviates was at 116 kPa, corresponding to inlet flow rates of 3.3×10^{-4} kg/s. During evaporation trials, although mass flow rates reached 4.0×10^{-4} kg/s, inlet pressures were approximately 105 kPa due to the absence of the rotameter. During validation measurements,

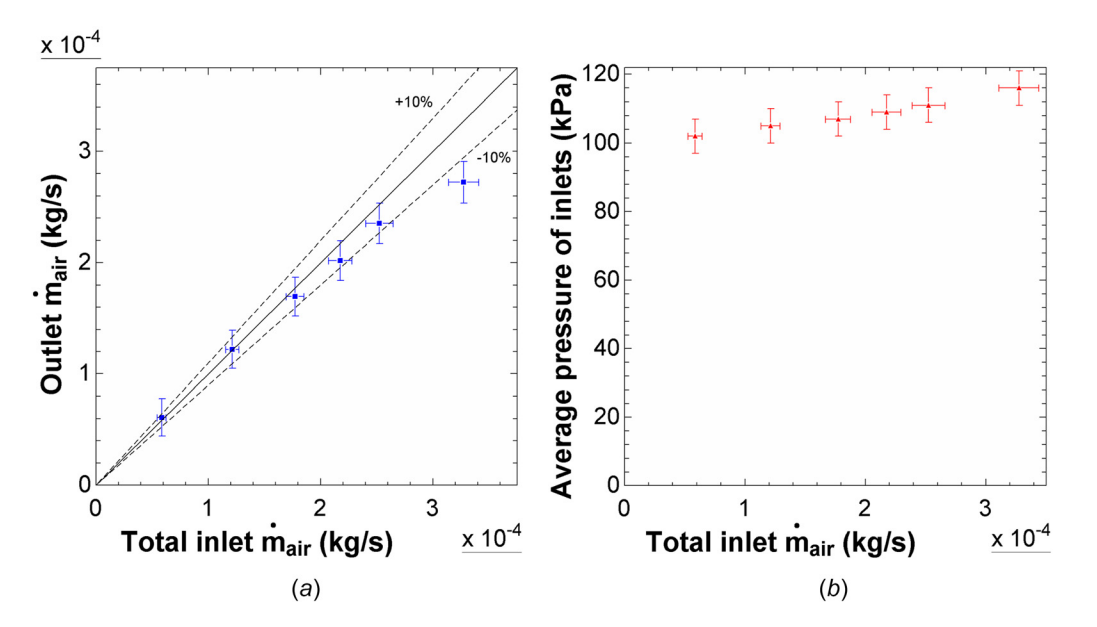


Fig. 5 Comparison of: (a) the mass flow rates through the test section and (b) the pressure variation with mass flow rates through the inlets. Data suggest pressure increase is not linear with increased inlet mass flow rates with the rotameter present.

pressures of 105 kPa were reached when inlet and outlet flows were both 1.7×10^{-4} kg/s.

3.2 Evaporation From Hydrophilic Ottawa Sand, the Hydrophobic Layer, and the Hydrophobic Mixture. Evaporation fluxes (i.e., evaporation rate was divided by the surface area of the sand layer (i.e., 0.19 m²); Fig. 6) differed between the three cases studied. The evaporation flux of all hydrophilic sand appears relatively high and constant from 37% saturation to 15% saturation, indicating the constant-rate evaporation period [14]. During this stage, capillary action within the sand pores brings moisture to the surface for evaporation by convection [10]. The reduction in evaporation flux at 12% saturation is the beginning of the falling-rate period, which Chakraborty et al. [6] attributed to the loss of the capillary connection of the water to the surface, and Shokri et al. [14] described as the point where the gravity and viscous resistance overcome the capillary forces. Once the saturation reached approximately 3%, there is negligible change in saturation and evaporation between trials, which suggests the slow-rate period had begun.

For the case with the 0.7-cm hydrophobic layer (i.e., 12% hydrophobic sand), the evaporation flux drops at approximately 20% saturation and falls to a quasi-steady evaporation flux from 18% to 6% saturation, before falling at 3% saturation. The initial reduction may be attributed to the hydrophilic layer above the hydrophobic material drying out, similar to the results of Shokri et al. [14]. Once the upper layer of the hydrophilic material was dry, the hydrophobic layer potentially suppresses evaporation by interrupting the capillary flow to the surface, thereby reducing the evaporation. This capillary interruption may be due to the water being repelled by the hydrophobic sand rather than adhering to it [31].

For the hydrophobic mixture (i.e., 12% hydrophobic material), the evaporation flux begins to fall at approximately 24% saturation and continues until dryout. Shokri et al. [19] determined that, in column experiments, as the percentage of mixed hydrophobic material increased, the length of the constant rate period decreased by disrupting the capillary forces driving water to the surface. Philip and De Vries [15] hypothesized that with a temperature gradient, condensation on one side and evaporation on the other side of liquid islands or bridges between particles increases evaporation by 3.6–18× compared to vapor diffusion predicted by Fick's law. Chakraborty et al. [6] suggested the liquid islands described by Philip and De Vries [15] (Fig. 7) form faster in hydrophilic pores, leading to the creation of the hydraulic connection and increased capillary action compared to hydrophobic pores. The presence of the

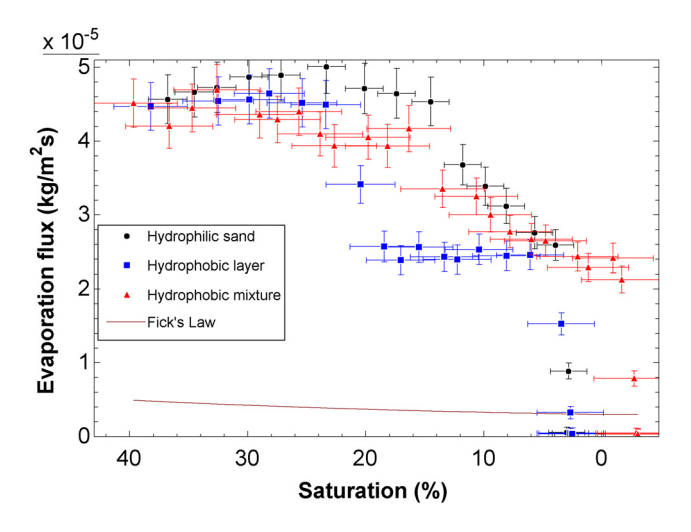


Fig. 6 Evaporative flux measured from the hydrophilic, hydrophobic layer, hydrophobic mixture experiments, and the corresponding diffusion flux calculated using Fick's law [14]

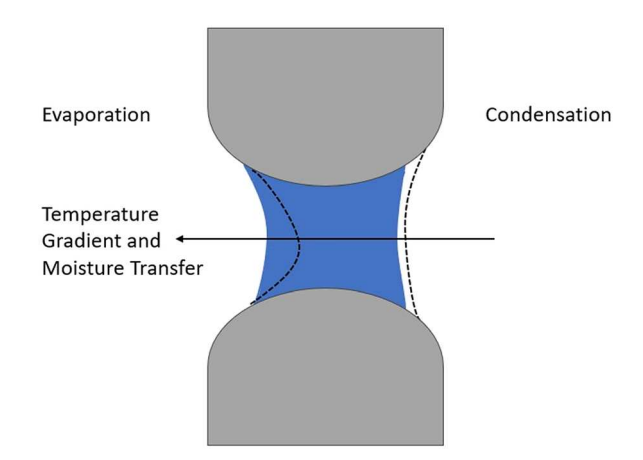


Fig. 7 Liquid island between two particles experiencing condensation and evaporation due to temperature gradient according to the theory of Philip and De Vries [15]

hydrophobic material may reduce liquid island formation and disrupt the capillary flow, as evidenced by the impediment of water entering the sand—water mixture during mixing, making it difficult to achieve the target saturation levels during sample preparation. The 12% hydrophobic mixture investigated in this work is similar to the 10% hydrophobic mixture used by Shokri et al. [19]; they attributed the decreased drying rate of the hydrophobic sand to the lack of hydraulic connections in the porous media. Dai et al. [45] also observed decreased capillarity in hydrophobic materials and evaporation enhancement in biphilic capillary channels, suggesting that hydrophilicity influences the curvature of the liquid interface and improves liquid supply while hydrophobicity reduces drag.

Figure 8 shows the all hydrophilic experiment remained at the highest evaporation rates for the longest period of saturation. At approximately 10% saturation, the all hydrophilic sand experiment had the highest evaporation rate, followed by the hydrophobic mixture, and the hydrophobic layer. The shortest constant-rate period was determined to be the hydrophobic mixture which began the falling-rate period of evaporation at the saturation of 24%, higher than the hydrophobic layer and hydrophilic sand which began the falling rate period at 20% and 12% saturation, respectively. It was also observed that the hydrophobic mixture had the longest falling rate period of the three cases. Reduced evaporation at lower saturations (e.g., drought conditions) is beneficial due to the time-value of water in an agricultural context; irrigation water holds a higher economic value when water is scarce, and it is less valuable immediately after a rainfall [8].

The saturation dropped minimally without forced flows over the course of 10 days in preliminary experiments, indicating that days between trials did not significantly alter the saturation; therefore, trial number was utilized as proxy variable (Fig. 8). The hydrophobic mixture experiment lasted 26 trials, compared to 17 trials for all hydrophilic sand and 20 trials for the hydrophobic layer. Figure 8(a) suggests that the hydrophobic mixture experiment had the shortest constant-rate period and reached lower evaporation rates at higher saturations compared to the other experiments which prolonged the overall experiment, similar to results of Shokri et al. [19].

3.3 Analysis of Vapor Diffusion of Water. The evaporative flux was compared to vapor diffusion flux calculated with Fick's law [6]

$$J = \frac{\theta_a^{2.5}}{n} D \frac{C_{\text{sat}} - C_{\infty}}{H(1 - S_{\text{tr}})}$$
 (11)

where J is the diffusive flux; θ_a is the volumetric air content; n is the porosity; D is the water-vapor diffusion coefficient (i.e.,

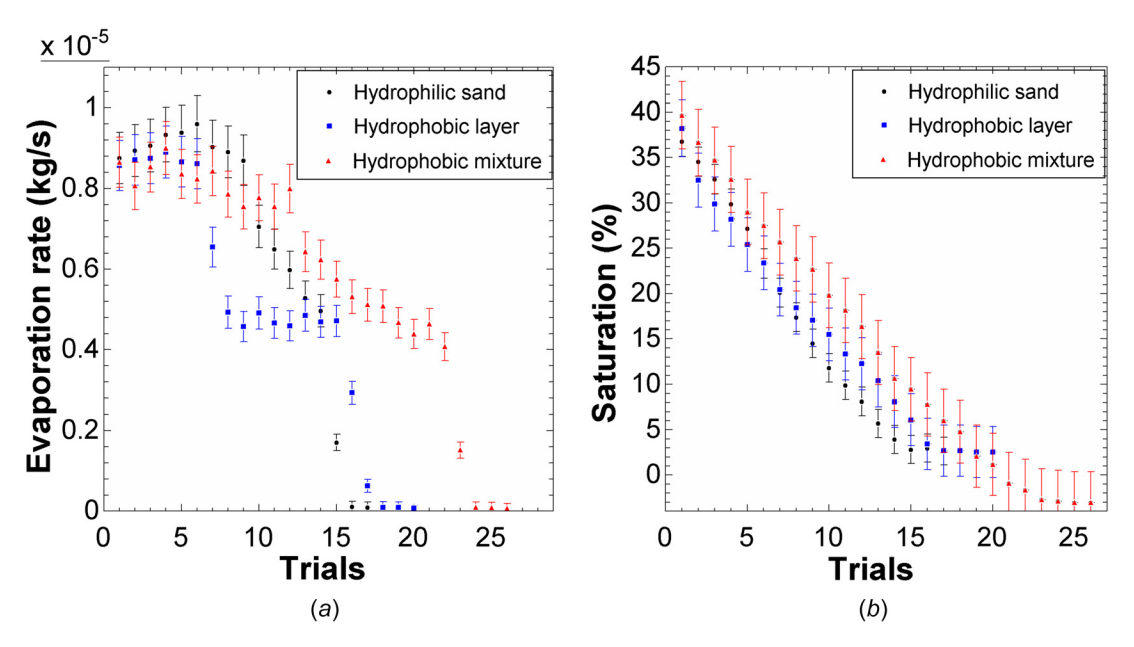


Fig. 8 The (a) evaporation rate and (b) saturation percentage for each trial of each experiment. Results indicate the hydrophobic mixture required the most trails to evaporate.

 2.73×10^{-5} m²/s at 30 °C [9]); $C_{\rm sat}$ and C_{∞} are the water-vapor densities at the evaporating interface and atmosphere, respectively; and H is the height of the sand layer (0.057 m). This equation assumes the concentration gradient of water in the sand is linear and the volumetric air content equals the porosity [6,14]. The waver-vapor densities were calculated using the saturated vapor partial pressure, $p_{\rm wrsat}$, and vapor partial pressure, $p_{\rm wr}$ [46]

$$RH = \frac{p_{wr}}{p_{wrsat}}$$
 (12)

where RH is the relative humidity of the air measured at the top inlet of the test section. The average sand temperature was $30\,^{\circ}\mathrm{C}$ for each experiment, which corresponded to a saturated vapor partial pressure of $4.246\,\mathrm{kPa}$ [46]. The relative humidity of the top inlet (i.e., near 0% RH) was used as it results in the largest difference in the water-vapor densities.

The evaporative fluxes for the three experiments are up to $12\times$ higher than the diffusion flux until the lowest saturation of each experiment is reached, suggesting that water vapor transport is enhanced compared to Fick's law, which only determines the slowrate period of evaporation [9]. The presence of liquid islands (Fig. 7) increases the hydraulic connection of water to the surface for evaporation in the hydrophilic and hydrophobic experiments, but form faster in the hydrophilic pores [6]. These liquid islands enhance the moisture transport from the sand compared to vapor diffusion, but likely form faster and remain longer in the hydrophilic experiment [6]. Both diffusion and the hydraulic connection of water to the top surface increase evaporation compared to diffusion alone [6]. These data suggest liquid island formation [15], capillary action [14], convective components [11], thermal gradients [16], and forced air flows through the sand increase evaporation and enhance vapor diffusion compared to Fick's law.

3.4 Analysis of Temperature Gradients Within the Sand Layer. As the solar heat flux was applied to the surface of the sand, a temperature gradient formed within the sand layer, which gave insight into heat transfer mechanisms. The temperature at location A, B, and C (0.079 m, 0.419 m, and 0.759 m, respectively) from the inlet to the test section at position 1, 2, and 3 (0.008 m, 0.02 m, and 0.035 m, respectively) below the surface were recorded (Fig. 9). Nonlinear coefficient of determination, R^2 values, indicate evaporative cooling. The R^2 values indicate linearity of the temperature

profile of the sand for various saturations (Table 1). At higher saturation percentages (i.e., 23–35%), for all experiments at inlet location A, the middle (position 2) thermocouple recorded a higher temperature than the near-surface (position) 1 thermocouple, suggesting that evaporative cooling is occurring near the inlet of the test section.

The temperature gradients at location B had higher R^2 values for saturations of 23–35% than at location A, suggesting there is still some evaporative cooling taking place at the surface of the sand for higher saturations, but there is less evaporation than at the inlet since the 0% RH at the inlet to the test section has the most capacity to evaporate water. As the relative humidity of the air increases, the evaporation potential of the air decreases and less evaporation occurs as the air progresses through the test section.

The temperature profiles for location C were linear for all saturations for the hydrophilic and hydrophobic mixture experiments, suggesting there is less evaporative cooling and higher values of relative humidity at this location. For the last saturation of each experiment, the R^2 values range 0.92–1 for all experiments, suggesting almost no evaporative cooling occurred (Table 1). The temperature profiles for the hydrophobic layer experiment and the hydrophobic mixture experiment had similar results; the hydrophobic layer experiment had R^2 values of 0.8 for the 9–12% saturation near the outlet to the test section, suggesting more evaporation was occurring compared to the all hydrophilic and hydrophobic mixture experiments. This suggests the hydrophobic layer is interrupting hydraulic connections [14] and reducing moisture transport from the soil leading to less evaporation near the inlet and center of the test section. A reduced evaporation rate would potentially lead to a lower relative humidity throughout the test section and more evaporation occurring at location C, leading to evaporative cooling and a lower R^2 value.

3.5 Fluid Flow and Heat Transfer Analysis With Dimensionless Numbers. Flow in the test section is modeled as a rectangular duct [47]

$$Re_{d_h} = \frac{\dot{m}_{a0}d_h}{\mu A_{\rm cross}} \tag{13}$$

$$d_h = \frac{4A_{\text{cross}}}{P_{\text{W}}} \tag{14}$$

$$x_{fd,h} \approx d_h(0.05 \operatorname{Re}_{d_h}) \tag{15}$$

where Re_{d_h} is the Reynolds number, μ is the dynamic viscosity, d_h is the hydraulic diameter of the flow area above the sand layer (0.056 m), A_{cross} is the cross-sectional area, Pw is the wetted perimeter, and the hydrodynamic entry length is $x_{fd,h}$. The average Reynolds number for each experiment was 83 and, thus, the flow is laminar. For these experiments, the entry length was 0.23 m, which is approximately a quarter of the length of the chamber. Nusselt numbers of 6.26 and 5.37 for uniform heat flux and surface temperature, respectively, are applicable for the aspect ratio of 7.2 in the test section. These Nusselt numbers are comparable to the Nusselt number of 5.39 for two flat plates with one side heated by a uniform heat flux and the other side insulated [48] (e.g., the test section is heated via the solar simulator from above and the sand acts as insulation below).

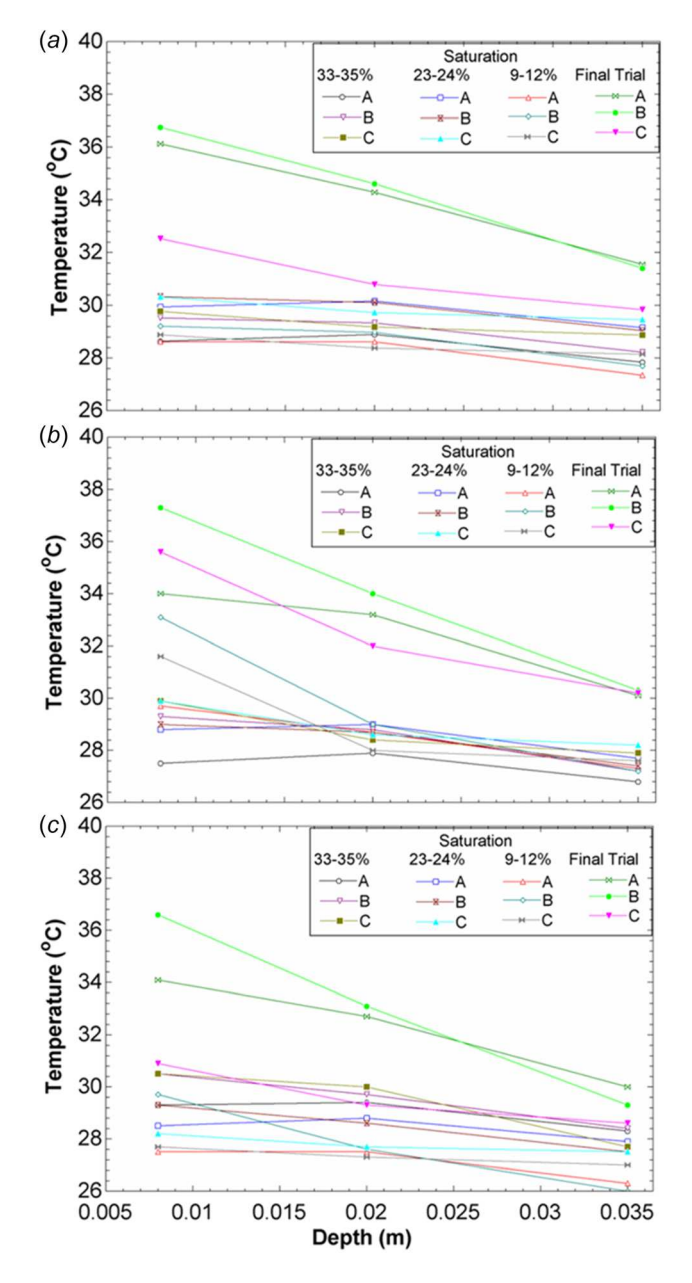


Fig. 9 Temperature profiles within the sand at locations A, B, and C for various saturations, in the (a) all hydrophilic, (b) hydrophobic layer, and (c) hydrophobic mixture experiments. Evaporative cooling at location A for 23–35% saturation leads to nonlinear temperature gradients.

Table 1 R^2 values for various saturation at each test section location showing linearity of the temperature gradient lines formed by graphing the temperatures at each depth in the sand

Saturation	33–35%	23–24%	9–12%	Final trial
All hydrophilic	experiment			
Location A	0.57	0.60	0.79	0.99
Location B	0.88	0.90	0.89	0.99
Location C	0.95	0.94	0.94	0.95
Hydrophobic la	aver experiment			
Location A	0.45	0.66	0.99	0.92
Location B	0.94	0.94	0.94	1
Location C	0.92	0.91	0.80	0.95
Hydrophobic n	nixture experime	ent		
Location A	0.71	0.50	0.76	0.98
Location B	0.99	0.99	0.99	1
Location C	0.96	0.94	0.95	0.95

The values of Reynolds number and Nusselt number were compared to studies conducted in a field, which model the surface as a flat plate (i.e., $Re_{L,cr} \sim 5.0 \times 10^5$). The comparison of the values of Reynolds and Nusselt numbers calculated in this study are compared to multiple field studies in areas that were deemed semi-arid climates (Table 2) [49–51], similar to the semi-arid region of the Central High Plains. Jacobs et al. [50] studied flows over a vineyard of bare and pruned grape vine stems in Castilla-La Mancha, Spain by measuring wind speed at 5.5 m and dry and wet bulb temperatures 6.0 m above the soil. In Niger, West Africa, Jacobs and Verhoef [51] measured mean wind speed and mean dry and wet bulb temperatures of fallow savanna at a height of 0.5 m above the soil. Gallego-Elvira et al. [49] measured the air temperature, relative humidity, and wind speed underneath a polyethylene mesh, but above a reservoir located in southeastern Spain. Each of the field studies measured temperatures within the range used for this study. The air velocities of the field studies are one to two orders of magnitude higher than the velocity of this study, and air did not pass through the porous media; however, the height of the velocity measurement is much larger than the boundary layer thickness. To perform a scale analysis across the studies, the ratio of boundary layer thickness, δ , (i.e., 0.016 m for this study) to the characteristic length, L, was calculated. The values calculated for this study are on the same order of magnitude as the field studies.

4 Conclusions

In this study, three evaporation experiments were performed on Ottawa sand with different wettabilities: (1) a completely hydrophilic layer of natural Ottawa sand, (2) a hydrophobic layer of Ottawa sand consisting of a 0.007-m-layer of coated hydrophobic Ottawa sand buried 0.018-m-below the surface (i.e., 12% hydrophobicity), and (3) a hydrophobic mixture of hydrophobic sand mixed into hydrophilic Ottawa sand (i.e., 12% hydrophobicity). Evaporation rates were measured using the conservation of mass of water on air flows entering and exiting the test section. Ottawa sand is naturally hydrophilic (contact angle of 23 deg), and the n-Octyltriethoxysilane coated Ottawa sand became hydrophobic with a contact angle of 109–117 deg.

This research suggests that mixed wettabilities (i.e., adding partial hydrophobicity to a hydrophilic porous media) may reduce the duration of the constant-rate evaporation period, thereby reducing the overall evaporation from a porous media and reducing water losses. The hydrophilic experiment lasted 17 trials and the falling-rate of evaporation began at 12% saturation, the hydrophobic layer experiment lasted 20 trails and the falling-rate began at 20% saturation, the hydrophobic mixture experiment lasted 26 trials and the falling-rate began at 24% saturation. Both experiments with hydrophobic material lasted longer than the all hydrophilic experiment and had shorter constant-rate periods, with the longest experiment and shortest constant-rate evaporation period occurring

Table 2 Calculated values of Reynolds, Nusselt, and Rayleigh number for this study and comparison to a field study

	Setting	Porous media	Re_L	Nu	$\frac{\delta}{L}$	Air temperature (°C)	u_{∞} (m/s)
Jacobs et al. [50]	Field study in Spain	Loamy-sand with stones	$2.0 \times 10^5 - 8.4 \times 10^5$	560–1690	0.006-0.011	10–30	0.1–7
Jacobs and Verhoef [51]	Field study in Niger, West Africa	Loamy-sand	$1.0 \times 10^5 - 8.7 \times 10^5$	140–1800	0.005-0.016	20–33	0.1–4
Gallego-Elvira et al. [49]	Field study in south-eastern Spain	Covered reservoir	$4.9 \times 10^5 - 8.7 \times 10^5$	3360–5590	0.005-0.007	27–34	0.18-0.32
Calculations for	this study using Re _{Dh} Setting	Media	Re_{Dh}	Nu	$rac{\delta}{L}$	Air temperature (°C)	u_{∞} (m/s)
This study	Laboratory	Ottawa sand	83	5.37-6.26	0.019	27.3–30.9	0.023

in the hydrophobic mixture. This suggests that the introduction of hydrophobic material interrupts capillary action of water to the soil surface and reduces evaporation. The introduction of hydrophobic material prolonged the experiment and decreased evaporation rates at higher saturations.

The measured evaporation flux for all periods of evaporation of each experiment was up to $12\times$ higher than the vapor diffusion flux calculated until the final trials of each experiment. The data suggest the formation of liquid islands within the sand enhanced vapor diffusion by creating a hydraulic connection and increased capillary action of the water to the surface of the sand, increasing evaporation compared to vapor diffusion alone [6,15]. Increased convection due to forced air flows through the sand layer also likely plays a role. The constant-rate and falling-rate periods of evaporation are not dependent on vapor diffusion [7]. The Reynolds and Nusselt numbers were calculated to be 83 and estimated to be 5.37–6.26, respectively, and the inclusion of both convection and solar heat flux components more closely represents field studies [49–51]. The values of δ/L for this study were also on the same order of magnitude as each field study.

Water was retained in the porous media for longer periods of time with the inclusion of hydrophobic particles in the hydrophilic, porous media. In an agricultural field, this would potentially reduce evaporation from the surface of soil. Mixed wettabilities would also allow water to penetrate the surface of the soil rather than creating runoff which occurs in all hydrophobic cases [20]. Mixing hydrophobic materials into soil can potentially be implemented into fields by way of tillage practices, which farmers currently use to alter the soil structure near the surface [5], thereby preventing a uniform layer of hydrophobic material and creating mixed wettabilities, similar to the hydrophobic mixture experiment. A uniform layer of hydrophobic material at the surface could potentially lead to surface runoff, thereby reducing the water penetration into the soil and water supply of the soil for crop use.

Future research could quantify the impacts of wettability on water retention and runoff in agricultural soils, as well as understand the impacts of different percentages of hydrophobic material and the impacts of different irrigation methods.

Acknowledgment

The authors would like to acknowledge the support of the CHIL Lab at Kansas State University. We would also like to thank Kyle Parr and Dr. Kulesza of Texas State University.

Funding Data

 The authors gratefully acknowledge the support of Directorate for Engineering, NSF (Grant No. 165141; Funder ID: 10.13039/100000084). Division of Graduate Education, NSF (Grant No. 1828571; Funder ID: 10.13039/100000082).

Data Availability Statement

The data and information that support the findings of this article are available in the following repository².

Nomenclature

 $A = \text{cross-sectional area (m}^2)$

 $C = \text{water-vapor density (kg/m}^3)$

d = diameter (m)

 $D = \text{diffusivity of water into air } (\text{m}^2/\text{s})$

e = void ratio

 $G_{\text{specific}} = \text{specific gravity}$

H = height of the sand layer (m)

 $J = \text{diffusion flux of water (kg/m}^2 \text{ s)}$

m = mass (kg)

 $\dot{m} = \text{mass flow rate (kg/s)}$

n = porosity

p = partial pressure of vapor (Pa)

Pw = wetted perimeter (m)

RH = relative humidity

S =saturation ratio t =time (s)

 $\dot{v} = \text{volumetric flow rate (m}^3/\text{s})$

 $w = \text{gravimetric water content } (kg_{\text{water}}/kg_{\text{sand}})$

x =entry length

Greek Symbols

 $\delta = \text{boundary layer thickness}$

 $\theta = \text{volumetric content}$

 $\mu = \text{dynamic viscosity (kg/ms)}$

 $\rho = \text{density (kg/m}^3)$

 $\omega = \text{humidity ratio } (\text{kg}_{\text{water}}/\text{kg}_{\text{air}})$

 Ω = denotes uncertainty of a variable

Nondimensional Numbers

Nu = Nusselt number

Re = Reynolds number

Subscripts

a = air

c = container

cr = critical

cross = cross-sectional

²https://data.mendeley.com/datasets/xw7shszjrk/1.

- fd,h = hydrodynamic
 - h = hydraulic
 - in = initial
 - L = characteristic length
 - s = sand
- sat = saturation
- tr = trial
- ts = test section
- u = uncertain
- wr = water
- 0 = top inlet to test section
- 1 = bottom inlet to test section
- 2 =outlet of test section
- $\infty = atmospheric$

References

- [1] University of Kansas Geological Survey, 2023, "Water in Kansas," University of Kansas, Lawrence, KS, accessed June 12, 2023, https://geokansas.ku.edu/waterkansas#:~:text=Almost%20all%20of%20the%20water,to%20pump%20the% 20groundwater%20out
- [2] K-State News, 2015, "Study Finds High Plains Aquifer Peak Use by State, Overall Usage Decline," Kansas State University, Manhattan, KS, accessed May 31, 2024, https://www.k-state.edu/media/newsreleases/nov15/aquifer111615.html
- [3] Kansas State University, 2020, "Kansas Climate," Kansas State University, Manhattan, KS, accessed June 12, 2023, https://climate.k-state.edu/basics/
- [4] McGuire, V. L., 2014, "Water-level changes and change in water in storage in the High Plains aquifer, predevelopment to 2013 and 2011-13," United States Geological Survey, Reston, VA, Report No. 2014-5218.
- [5] Ochsner, T., Howerton, E., and Ellis, B., 2019, "Rain or Shine," Oklahoma State University, Stillwater, OK.
- [6] Chakraborty, P. P., Ross, M., Bindra, H., and Derby, M. M., 2022, "Evaporative Drying From Hydrophilic or Hydrophobic Homogeneous Porous Columns: Consequences of Wettability, Porous Structure and Hydraulic Connectivity," Transp. Porous Media, 143(3), pp. 551–578.
- [7] Qiu, G. Y., and Ben-Asher, J., 2010, "Experimental Determination of Soil Evaporation Stages With Soil Surface Temperature," Soil Sci. Soc. Am. J., 74(1), pp. 13–22.
- [8] Gutierrez, M. M., Cameron-Harp, M. V., Chakraborty, P. P., Stallbaumer-Cyr, E. M., Morrow, J. A., Hansen, R. R., and Derby, M. M., 2022, "Investigating a Microbial Approach to Water Conservation: Effects of Bacillus Subtilis and Surfactin on Evaporation Dynamics in Loam and Sandy Loam Soils," Front. Sustainable Food Syst., 6, p. 441.
- [9] Hillel, D., 1998, Environmental Soil Physics, Academic Press, Waltham, MA.
- [10] Gupta, B., Shah, D., Mishra, B., Joshi, P., Gandhi, V. G., and Fougat, R., 2015, 'Effect of Top Soil Wettability on Water Evaporation and Plant Growth," J. Colloid Interface Sci., 449, pp. 506-513.
- [11] Davarzani, H., Smits, K., Tolene, R. M., and Illangasekare, T., 2014, "Study of the Effect of Wind Speed on Evaporation From Soil Through Integrated Modeling of the Atmospheric Boundary Layer and Shallow Subsurface," Water Resour. Res., **50**(1), pp. 661–680.
- [12] Knappett, J., and Craig, R. F., 2012, Craig's Soil Mechanics, CRC Press, Boca Raton, FL.
- [13] An, N., Tang, C.-S., Xu, S.-K., Gong, X.-P., Shi, B., and Inyang, H. I., 2018, "Effects of Soil Characteristics on Moisture Evaporation," Eng. Geol., 239, рр. 126–135.
- [14] Shokri, N., Lehmann, P., and Or, D., 2008, "Effects of Hydrophobic Layers on Evaporation From Porous Media," Geophys. Res. Lett., 35(19), p. L19407.
 [15] Philip, J., and De Vries, D. D., 1957, "Moisture Movement in Porous Materials
- Under Temperature Gradients," EOS, Trans. Am. Geophys. Union, 38(2), pp. 222–232.
- [16] Cary, J., 1963, "Onsager's Relation and the Non-Isothermal Diffusion of Water Vapor," J. Phys. Chem., 67(1), pp. 126–129.
 [17] Jury, W., and Letey Jr, J., 1979, "Water Vapor Movement in Soil: Reconciliation
- of Theory and Experiment," Soil Sci. Soc. Am. J., 43(5), pp. 823-827.
- [18] Chakraborty, P. P., Huber, R., Chen, X., and Derby, M. M., 2018, "Evaporation From Simulated Soil Pores: Effects of Wettability, Liquid Islands, and Breakup," Interfacial Phenom. Heat Transfer, 6(4), pp. 391-407.
- [19] Shokri, N., Lehmann, P., and Or, D., 2009, "Characteristics of Evaporation From Partially Wettable Porous Media," Water Resour. Res., 45(2), p. W02415.
- [20] DeBano, L. F., 1981, Water Repellent Soils: A State-of-the-Art, U.S. Department of Agriculture, Forest Service, Pacific Southwest Forest and Range Experiment Station, Berkeley, Calif.
- [21] Doerr, S. H., Shakesby, R., and Walsh, R., 2000, "Soil Water Repellency: Its Causes, Characteristics and Hydro-Geomorphological Significance," Earth-Sci. Rev., **51**(1–4), pp. 33–65.

- [22] Bachmann, J., Woche, S., Goebel, M. O., Kirkham, M., and Horton, R., 2003, "Extended Methodology for Determining Wetting Properties of Porous Media," Water Resour. Res., 39(12), p. SBH11.
- [23] Ellerbrock, R., Gerke, H., Bachmann, J., and Goebel, M.-O., 2005, "Composition of Organic Matter Fractions for Explaining Wettability of Three Forest Soils," Soil Sci. Soc. Am. J., 69(1), pp. 57–66.
- [24] Jaramillo, D., Dekker, L., Ritsema, C., and Hendrickx, J., 2000, "Occurrence of Soil Water Repellency in Arid and Humid Climates," J. Hydrol., 231-232, pp. 105-111.
- [25] Morley, C., Mainwaring, K., Doerr, S., Douglas, P., Llewellyn, C., and Dekker, L., 2005, "Organic Compounds at Different Depths in a Sandy Soil and Their Role in Water Repellency," Soil Res., 43(3), pp. 239–249.
- [26] Wallis, M., and Horne, D., 1992, "Soil Water Repellency," Adv. Soil Sci., 20, pp.
- [27] Certini, G., 2005, "Effects of Fire on Properties of Forest Soils: A Review," Oecologia, 143(1), pp. 1-10
- [28] Cerdà, A., and Doerr, S. H., 2007, "Soil Wettability, Runoff and Erodibility of Major Dry-Mediterranean Land Use Types on Calcareous Soils," Hydrol. Processes: Int. J., 21(17), pp. 2325–2336.
- [29] Booker, F., Dietrich, W., and Collins, L., 1993, "Runoff and Erosion After the
- Oakland Firestorm," Calif. Geol., 46(6), pp. 159–173.
 [30] Da Re, G., Germaine, J. T., and Ladd, C. C., 2001, "Physical Mechanisms Controlling the Pre-Failure Stress-Strain Behavior of Frozen Sand," Massachusetts Institute of Technology, Cambridge, MA.
- [31] Truong, Q. H., Lee, J.-S., Dong, Y., and Yun, T. S., 2011, "Capillary Induced Small-Strain Stiffness for Hydrophilic and Hydrophobic Granular Materials: Experimental and Numerical Studies," Soils Found., 51(4), pp. 713–721
- [32] Tester, M., and Morris, C., 1987, "The Penetration of Light Through Soil," Plant, Cell Environ., 10(4), pp. 281–286.
- [33] Baranoski, G. V., Kimmel, B. W., Varsa, P., and Iwanchyshyn, M., 2019, "On the Light Penetration in Natural Sands," Proceedings of the IGARSS 2019-2019 IEEE International Geoscience and Remote Sensing Symposium, Yokohama, Japan, July 28-Aug. 2, pp. 6933-6936.
- [34] Humboldt, 2024, "Humboldt: Ottawa Test Sand for Cube Molds," Humboldt, Elgin, IL, accessed Oct. 15, 2022, https://www.humboldtmfg.com/ottawa-testsand.html
- [35] McGaw, R., 1968, "Thermal Conductivity of Compacted Sand/Ice Mixtures," Highway Research Record, Highway Research Board, Hanover, NH.
- [36] Tarnawski, V. R., Momose, T., Leong, W., Bovesecchi, G., and Coppa, P., 2009, "Thermal Conductivity of Standard Sands-Part I. Dry-State Conditions," Int. J. Thermophys., 30(3), pp. 949–968. Kersten, M. S., 1949, "Thermal Properties of Soils," University of Minnesota,
- Minneapolis, MN.
- [38] Ratliff, L., Ritchie, J., and Cassel, D., 1983, "Field-Measured Limits of Soil Water Availability as Related to Laboratory-Measured Properties," Soil Sci. Soc. Am. J., 47(4), pp. 770-775
- [39] Robichaud, P., and Hungerford, R., 2000, "Water Repellency by Laboratory Burning of Four Northern Rocky Mountain Forest Soils," J. Hydrol., 231-232, pp. 207–219.
- [40] Hillel, D., 2013, Fundamentals of Soil Physics, Academic Press, Waltham, MA.
- [41] Bastidas, A. M. P., 2016, Ottawa F-65 Sand Characterization, University of California, Davis, CA.
- [42] El Ghoraiby, M., Park, H., and Manzari, M. T., 2020, "Physical and Mechanical Properties of Ottawa F65 Sand," Model Tests and Numerical Simulations of Liquefaction and Lateral Spreading: LEAP-UCD-2017, pp. 45-67.
- [43] Kutter, B. L., Manzari, M. T., and Zeghal, M., 2019, Model Tests and Numerical Simulations of Liquefaction and Lateral Spreading: LEAP-UCD-2017, Springer Nature, New York
- [44] Kine, S. J., and McClintock, F. A., 1953, "Describing Uncertainties in Single-Sample Experiments," Mech. Eng., 75(1), pp. 3–8.
- [45] Dai, X., Yang, F., Yang, R., Huang, X., Rigdon, W. A., Li, X., and Li, C., 2014, "Biphilic Nanoporous Surfaces Enabled Exceptional Drag Reduction and Capillary Evaporation Enhancement," Appl. Phys. Lett., 105(19), p. 191611.
- [46] Moran, M. J., Shapiro, H. N., Boettner, D. D., and Bailey, M. B., 2010, Fundamentals of Engineering Thermodynamics, Wiley, Hoboken, NJ.
- [47] Bergman, T. L., Bergman, T. L., Incropera, F. P., Dewitt, D. P., and Lavine, A. S., 2011, Fundamentals of Heat and Mass Transfer, Wiley, Hoboken, NJ.
- [48] Bejan, A., 2013, Convection Heat Transfer, Wiley, Hoboken, NJ.
- [49] Gallego-Elvira, B., Baille, A., Martín-Gorriz, B., Maestre-Valero, J. F., and Martínez-Alvarez, V., 2012, "Evaluation of Evaporation Estimation Methods for a Covered Reservoir in a Semi-Arid Climate (South-Eastern Spain)," J. Hydrol., 458-459, pp. 59-67.
- [50] Jacobs, A., Verhoef, A., and de Bruin, H., 1996, "Sensible Heat Flux From Sparse Vegetation Estimated Using Nusselt Numbers," Phys. Chem. Earth, 21(3),
- [51] Jacobs, A. F., and Verhoef, A., 1997, "Soil Evaporation From Sparse Natural Vegetation Estimated From Sherwood Numbers," J. Hydrol., 188-189, pp. 443-452.